J Neurophysiol 108: 215–226, 2012.
First published April 11, 2012; doi:10.1152/jn.00710.2011.

Reduction in receptive field size of macaque MT neurons in the presence of visual noise

Hironori Kumano and Takanori Uka
Department of Neurophysiology, Graduate School of Medicine, Juntendo University, Bunkyo, Tokyo, Japan

Submitted 29 July 2011; accepted in final form 6 April 2012

Kumano H, Uka T. Reduction in receptive field size of macaque MT neurons in the presence of visual noise. *J Neurophysiol* 108: 215–226, 2012. First published April 11, 2012; doi:10.1152/jn.00710.2011.—The visual system faces a trade-off between increased spatial integration of disparate local signals and improved spatial resolution to filter out irrelevant noise. Increased spatial integration is beneficial when signals are weak, whereas increased spatial resolution is particularly beneficial when focusing on a small object in a cluttered natural scene. The receptive field (RF) size of visual cortical neurons can be modulated depending on various factors such as sensory context, allowing adaptive integration of sensory signals. In this study, we explored the spatial integration properties of neurons in macaque middle temporal visual area (MT). We hypothesized that spatial resolution would increase when high-contrast noise was presented simultaneously with a visual stimulus, enabling focus on a small object in a cluttered scene. To test this hypothesis, we mapped the RFs of MT neurons of two fixating monkeys in a 5 × 5 grid manner using a small patch of random-dot motion. To examine the effects of noise on RF profile, a dynamic noise (0% coherence dots) of varying diameter was concurrently presented at the RF center. We found that RF size decreased when noise diameter increased. Analyses based on the response normalization model and area summation provided evidence for the potential contribution of spatial summation properties within the RF and surround suppression to the apparent contraction of RF size. Our results suggest that MT neurons integrate smaller regions of motion signals when signals are embedded in noise, an efficient strategy to filter out surrounding noise.

middle temporal area; surround suppression; response normalization

IN THE PRIMATE VISUAL CORTEX , information is first represented by neurons in the primary visual cortex (V1). Because V1 neurons can only signal the stimulus energy within their spatiotemporal pass-band in the small receptive field (RF), local signals from diverse V1 neurons must be spatially integrated to create a unified visual percept. Neurons in extrastriate visual areas with large RFs are well suited for spatial integration of distributed local signals.

Spatial integration, on the one hand, can improve the signal-to-noise ratio by averaging out noise when the signal is weak. Conversely, this comes at the expense of spatial resolution; details within the averaged region are lost due to integration. The visual system thus faces a trade-off. Specifically, larger regions of integration are desirable for the reliability of the signal, but fine spatial details require smaller regions of integration (Lombrozo et al. 2005). Although the optimal solution to this trade-off should depend on viewing environments, the RF extent of neurons places a limit on the spatial resolution of visual processing.

When a signal is weak (e.g., low contrast), substantial integration across space is needed at the cost of spatial resolution. Indeed, spatial summation of V1 neurons is affected by stimulus contrast; the area of spatial summation increases with a decrease in contrast (Kapadia et al. 1999; Sceniak et al. 1999; Cavanaugh et al. 2002). This demonstrates a strategy of the visual system to enhance sensitivity to weak sensory signals. In the case of visual motion, the strength of motion can be controlled by using stochastic random-dot motion (Morgan and Ward 1980). Using these stimuli, Hunter and Born (2011) demonstrated that reducing the strength of motion increased surround suppression of neurons in the middle temporal area (MT), suggesting that reduction of stimulus strength does not necessarily induce an increase in spatial integration. The increased surround suppression (i.e., the reduced spatial integration) for low motion coherence stimuli seems to be disadvantageous when processing spatially uniform motion signals. However, for natural scenes containing signals surrounded by noise, this characteristic may be advantageous for filtering out irrelevant noise. This raises the possibility of an improvement of spatial resolution by apparent contraction of RF size.

In this study, we examined this hypothesis for MT neurons by applying a method different from Hunter and Born (2011), the minimum-response-field (MRF) method in which the RF is delineated as the portion of the visual field where a small stimulus evokes excitatory responses from the neuron. We mapped the RFs of individual MT neurons while simultaneously presenting a high-contrast noise of varying diameter. Consistent with Hunter and Born (2011), we found that the apparent size of the RF of individual MT neurons contracted when presented with large visual noise within and around the RF. Our results suggest that MT neurons change their spatial resolution depending on the amount of noise.

MATERIALS AND METHODS

The general experimental procedures were identical to those described previously (Uka and DeAngelis 2003; Kumano and Uka 2010). Here, we briefly summarize aspects relevant to the present study. All animal care, training, and experimental procedures were in accordance with the National Institutes of Health's guidelines and were approved by the Juntendo University Animal Care and Use Committee.

Subjects and surgery. We used two Japanese macaque monkeys (*Macaca fuscata*): one female (*monkey P*; 6 kg) and one male (*monkey K*; 8 kg). Animals were prepared for experiments using standard aseptic surgeries. A post for head restraint and a recording chamber were chronically implanted in each monkey. To monitor eye movements, we implanted scleral search coils into both eyes for *monkey P*

Address for reprint requests and other correspondence: T. Uka, Dept. of Neurophysiology, Graduate School of Medicine, Juntendo Univ., 2-1-1 Hongo, Bunkyo, Tokyo 113-8421, Japan (e-mail: uka@juntendo.ac.jp).

0022-3077/12 Copyright © 2012 the American Physiological Society

and one eye for *monkey K* (Judge et al. 1980). A cylindrical recording chamber was mounted over the occipital cortex ~17 mm lateral and 14 mm dorsal to the occipital ridge at an angle of 25° above the horizontal. Area MT was accessed by passing through the striate cortex and extrastriate visual areas in the lunate sulcus.

Tasks and visual stimuli. The behavioral task and data acquisition were controlled by a commercial software package (TEMPO; Reflective Computing, Olympia, WA). The monkeys were seated and head-restrained in a primate chair. A DLP projector (Mirage S+2K; Christie Digital Systems, Ontario, Canada) back-projected a visual stimulus on a tangent screen positioned 57 cm in front of the monkeys' eyes. The screen subtended a visual angle of 122° × 91°. Stimuli were presented dichoptically using a pair of ferro-electric liquid crystal shutters (DisplayTech, Longmont, CO) that were mounted just in front of the monkeys' eyes. Stereo half-images for the left and right eyes were presented alternately at a frame rate of 100 Hz (i.e., 50-Hz refresh for each eye) and were synchronized with the vertical refresh of the video input. This study, however, did not investigate stereoscopic processing, and thus all stimuli were presented at the preferred disparity (see below). The monkeys viewed random-dot stimuli while maintaining fixation on a yellow dot (0.15°) on the screen. The monkeys received a drop of water as a reward when their conjugate eye position remained within a 2.0° × 2.0° electronic window around the fixation point during stimulus presentation (500 ms). If the monkeys broke fixation during the trial, the trial was terminated, the data were discarded, and the monkeys were not rewarded.

Random-dot stimuli were presented using an OpenGL accelerator board with quad-buffer stereo support (Quadro FX 1400; NVIDIA, Santa Clara, CA). Each random-dot stereogram (RDS) was presented within a circular aperture. Dot density was 64 dots per square degree per second, with each dot subtending ~0.1°. The starting position of each dot was newly randomized for each trial. The RDS consisted of red dots (5.3 cd/m^2) presented on a black background (0.10 cd/m^2). Precise binocular disparities and smooth motion were achieved by plotting dots with subpixel resolution using antialiasing provided by the OpenGL board.

Electrophysiological recordings. We used a tungsten microelectrode (FHC, Bowdoin, ME) with impedance values between 0.5 and 2.0 MΩ (at 1 kHz) for recording the extracellular activity of single neurons. The electrode was advanced through the cortex through a transdural guide tube using a pulse motor micromanipulator (MO-951; Narishige, Tokyo, Japan) mounted on the recording chamber. Raw signals from the electrode were amplified and bandpass filtered (200–10000 Hz) with conventional electronic equipment (Bak Electronics, Mount Airy, MD). We isolated single neurons using a voltage-time window discriminator (Bak Electronics). Times of action potential and trial event occurrences were stored to a disk with 1-ms resolution. Eye position was monitored using a magnetic search coil system (Sankeikizai, Tokyo, Japan) and stored to a disk at a rate of 250 Hz. Area MT was identified based on interpreting the pattern of gray matter and white matter encountered during electrode penetration and on the physiological response properties (direction, speed, horizontal disparity tuning, receptive field location, and size) of both single neurons and multiunit clusters.

Experimental protocols. After isolating a single MT neuron, we qualitatively explored RF size and location, as well as tuning properties (direction, speed, and horizontal disparity) of the neuron using a small circular patch of coherently moving random dots. Next, we conducted a set of quantitative preliminary tests to measure speed tuning, horizontal disparity tuning, RF size and location, size tuning (area summation), and direction tuning of each MT neuron. Each of these measurements was performed in a separate block of randomly interleaved trials, with each unique stimulus presented at least three times. During these tests, a tuning curve or RF map was constructed online, and the preferred stimulus parameter was used in subsequent tests. First, speed tuning was measured by presenting dots that drifted at 0, 1, 2, 4, 8, 16, 32, and 64°/s. Horizontal disparity tuning was then measured at the preferred speed by presenting dot patterns the horizontal disparity of which varied from −1.6° to 1.6° in steps of 0.4°. Next, we mapped the RF by presenting a small (~0.25 × approximate RF diameter) patch of random dots drifting at the preferred speed and horizontal disparity at each location on a 4 × 4 grid that covered the entire RF. A two-dimensional (2-D) Gaussian function with an identical radius along two cardinal axes was fit to this RF map. This test was designed to obtain quantitative estimates of the RF center and radius (σ of the fitted Gaussian function), which were used for the main experiment. After determining the RF center, we assessed size tuning by presenting dots within circular apertures at the RF center. We presented aperture sizes of 1, 2, 4, 8, 16, 32, and 64° in diameter. Subsequently, direction tuning was measured by presenting eight motion directions, 45° apart, with all other parameters optimized.

Examination of effects of noise diameter on RF structures. Following the preliminary tests, we obtained a finer-scale RF map under various noise conditions. For this experiment, a virtual 5 × 5 grid was positioned at the RF center (Fig. 1). For each trial, a small circular patch of random dots (probe) drifting in either the preferred or opposite (null) direction was presented at each grid location. For a subpopulation (47 of 135 neurons), we only used the preferred direction for this test. The speed and the horizontal disparity of the probe were kept at the preferred values. The probe diameter was half the RF radius, derived as the σ of the 2-D Gaussian fitted to the initial 4 × 4 RF map. The grid spacing was a unit σ from the fitted 2-D Gaussian function. Thus the full mapping range covered 4.5 × the RF radius. Using these parameters, we have succeeded in accurately estimating the size and position of RFs of MT neurons (Kumano and Uka 2010). To examine the effects of noise on RF profiles, a noise patch in which all dots were randomly replotted every fourth video frame (i.e., 0% coherence) was concurrently presented at the estimated RF center. The horizontal disparity of the noise patch was the same as the probe. For each neuron, we predetermined a set of three or four different noise diameters chosen from the following values: 0, 0.8, 1.6, 3.2, 6.4, and 12.8 × σ degrees in visual angle. During the experimental run, on each trial, we selected one noise diameter from the predetermined set and presented the noise patch of that diameter. The probe and the noise patch were not transparent, and the probe overrode the noise patch when the two overlapped. We always

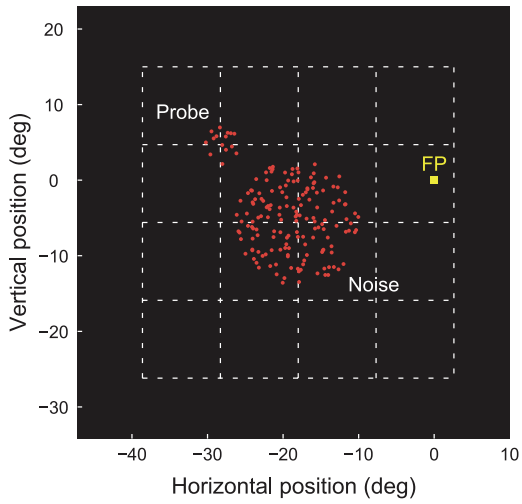

Fig. 1. Schematic illustration of the receptive field (RF) mapping procedure. While monkeys fixated on the fixation point (FP; yellow square), a small circular patch of fully coherent moving dots (probe) was presented at 1 of 25 positions configured in a 5 × 5 grid. Grid position, grid size, and probe size were determined from an initial crude mapping of the RF of a middle temporal visual area (MT) neuron under study. A circular patch of 0% coherent moving dots (noise) was also presented at the RF center. Diameter of the noise patch was varied across trials to examine the effects of noise on the RF structure.

included a no noise (i.e., $0 \times \sigma$) condition to quantitatively compare differences in RF profiles with and without noise. Data were discarded if neural isolation was lost before three repetitions. The median number of trial repetitions across the range of accepted data sets was 10 (5.3 SD).

In an additional experiment, we used transparent probe and noise patches. Other experimental procedures were identical to the original experiment. Dot density of the region of the probe patch was slightly lower than 128 ($=64 \times 2$) dots per square degree per second, because the dots of the probe and those of noise could overlap. The median number of trial repetitions across the range of this additional experiment was 7 (2.2 SD).

Data analysis. Neuronal responses to each stimulus condition were defined as the mean firing rate across trial repetitions in the time window of visual stimulus duration. Spontaneous firing rate was calculated from spiking activity during presentation of a blank screen.

The confidence interval of the extracted RF parameters, such as the RF size (see Fig. 4*A*), was calculated by bootstrap resampling (Efron 1979). A hypothetical data set was generated by independent random sampling with replacement from the original firing rates under particular stimulus conditions. The RF map was generated from the hypothetical data set, and this procedure was repeated 1,000 times. Derived quantities were calculated for each of 1,000 resampled RFs, and the 2.5 and 97.5 percentiles of the 1,000 values were used as an estimate of the 95% confidence interval.

We assessed whether each MT neuron had an inhibitory surround by fitting the size-tuning curve with two models: a single error function (erf, the integral of a Gaussian) model and a difference of error (DoE) function model (Raiguel et al. 1995; DeAngelis and Uka 2003; Tsui and Pack 2011). The former model provided good fits to size-tuning curves for neurons that lacked surround suppression and is given by the following equation:

$$R(w) = R_0 + A_e \times erf\left(\frac{w}{a}\right) \quad (1)$$

where w, A_e, a, and R_0 are the diameter of the stimulus, the excitatory amplitude, the size of the excitatory RF, and the spontaneous firing rate (the response to zero size), respectively. The DoE model incorporates the subtractive interaction between the center and surround mechanisms and is given by:

$$R(w) = R_0 + A_e \times erf\left(\frac{w}{a}\right) - A_i \times erf\left(\frac{w}{b}\right) \quad (2)$$

where A_i and b ($> a$) are the amplitude and the size of the suppressive surround mechanism. The errors of these fits were compared using a sequential F test. If the DoE model provided a significantly better fit than the single error function model ($P < 0.05$), the neuron was considered to have an inhibitory surround.

For each size-tuning curve, we computed the percentage of surround suppression as:

$$\%\ \text{Surround Suppression} = 100 \times \left(\frac{R_{opt} - R_{largest}}{R_{opt}}\right) \quad (3)$$

where R_{opt} is the response at the optimal size (determined from the curve fit) and $R_{largest}$ is the response to the largest size (Tsui and Pack 2011). This metric was always computed from the DoE model fit.

In the analysis of the transparent probe/noise patch experiment data, we addressed whether spatial summation properties within the RF can account for our results. Specifically, using the responses to the probe and the noise patch presented individually, we predicted the responses to the simultaneous presentation of probe and noise using a spatial summation model. We then examined whether the model reproduced the experimentally observed RF profile when presented with noise patches. The model is a generalized nonlinear summation model that has been used to examine spatial summation properties for neurons in area MT (Britten and Heuer 1999; Heuer and Britten 2002) and other areas (Ghose and Maunsell 2008; Oleksiak et al. 2011). The model is expressed as follows:

$$R = a\left[\left(r_{probe}\right)^n + \left(r_{noise}\right)^n\right]^{1/n} + b \quad (4)$$

where r_{probe} and r_{noise} denote the responses to the probe and the noise patch presented individually. R is the response to the probe and noise patch presented simultaneously. The two parameters of the model, the scale factor, a and the exponent, n control the spatial summation characteristics, from averaging ($a = 0.5$, $n = 1$) to winner-take-all ($a = 1$, large n), and b is the intercept. As in Britten and Heuer (1999), we fit various versions of this model, described in detail in RESULTS, by minimizing the sum of squared errors between the neuronal responses and R, using the constrained minimization tool, fmincon, in MATLAB (Mathworks). We evaluated the quality of model fit by calculating the variance in mean firing rates accounted for by the model (R^2 values).

RESULTS

We recorded from a total of 135 neurons from two monkeys (93 from *monkey K* and 42 from *monkey P*). The eccentricities of recorded neurons ranged from 3.6 to 31.0°. The RFs of MT neurons were mapped at a 5×5 resolution while a noise patch of various diameters was simultaneously presented (Fig. 1). Of the 135 neurons, 88 (46 from monkey K and 42 from monkey P) were available for RF maps for both the preferred and null direction. We first quantified RF parameters such as amplitude and size and determined the effects of noise diameter on these parameters. We then calculated neuronal performance in motion-direction discrimination and examined the effects of noise diameter on neuronal performance.

Effects of visual noise on RF profiles of MT neurons. Figure 2 illustrates results obtained from an example MT neuron. Raw RF maps were compiled for each noise condition as a set of colored circles, with a color denoting mean firing rates at each grid location (Fig. 2 *A–D*). For this particular neuron, we selected noise diameter values to be 0, 0.8, 1.6, and $3.2 \times$ the RF radius. The estimate of the RF center and the RF radius (the center position and σ of a 2-D Gaussian fit) from the initial RF mapping using 4×4 resolution was (−18.0° and −5.6°) and 10.3°, respectively. Thus the examined noise diameter ranged from 8.2 to 33.0°, as shown in Fig. 2, *A-D*, whereas the probe dot aperture was 5.15° in diameter (half the RF radius). Note that the RF maps under noise presentation (Fig. 2, *B–D*) were constructed from responses to both the probe patch presented at the respective grid positions and the noise patch presented at the RF center. From these raw RF maps, we used cubic spline interpolation to create a "spline RF map," as shown in Fig. 2, *E–H*. The color scales of responses are identical across *A–H*. Inspection of these spline RF maps indicates that when presented with larger noise patches, the extent of the apparent RF (brighter area in the spline RF maps) contracted, and the response at the RF center decreased.

The RF maps obtained with the null direction in this example neuron are shown in Fig. 3. As for the preferred direction, spline RF maps (Fig. 3, *E–H*) for the null direction were constructed from raw RF maps (Fig. 3, *A–D*). For this neuron, the RF map for the null direction without noise showed a "doughnut-like" profile, i.e., a region of weak responses was surrounded by a region of modest responses (Fig. 3*E*). When presented with noise patches, the null RF maps showed no coherent structure (Fig. 3, *F–H*).

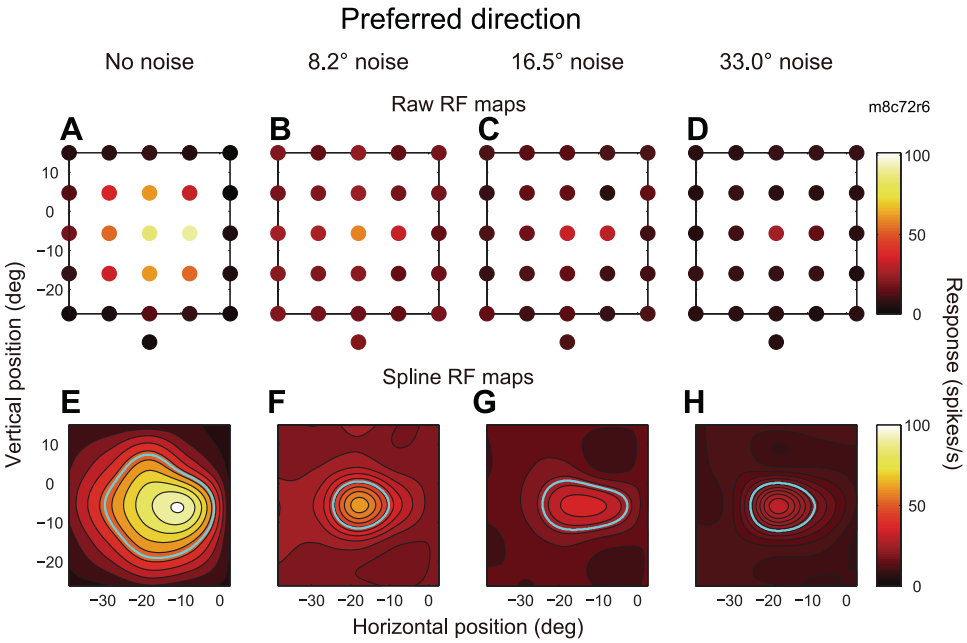

Fig. 2. An example MT neuron showing contraction of the apparent RF size when presented with noise. *A–D*: raw RF maps for the preferred direction are compiled as a set of colored circles, with a color denoting mean firing rates as indicated by the color bar. Noise-patch diameters are written on the top of each RF map. Colored circles below the raw RF maps indicate responses to the noise patch. *E–H*: smooth maps of the RF surface were created by interpolating the raw RF maps with a two-dimensional (2-D) cubic spline function. Cyan lines are the circumference of the RF area that exceeds half the peak-response modulation. Color scales of the RF map responses are identical across *A–H*.

To quantify the effects of noise on apparent RF sizes for the preferred direction, we first calculated the response modulation at each grid location by subtracting responses to the noise patch alone from responses to the probe patch (the noise patch was also presented). The RF area was then defined as the area of the spline RF map that exceeded half the largest response modulation (as in Womelsdorf et al. 2008), the circumference of which is denoted by cyan lines in Fig. 2, *E–H*. When different sizes of noise patches were presented, the apparent RF sizes contracted compared with that without a noise patch. The RF size was calculated as the square root of the RF area, and the RF size for this example neuron is plotted as a function of the diameter of the noise patch in Fig. 4*A*. The RF size of this neuron without a noise patch was 23.0° (see Fig. 2*E*). When a noise of 8.2° was presented, the RF size contracted to 11.5°. With larger noises, the RF sizes were variable, but remained contracted (Fig. 4*A*; 14.5 at 16.5° noise and 12.6 at 33.0° noise).

The response at the RF center for the preferred direction of this neuron monotonically decreased when larger noise was presented (Fig. 4*B*, filled circle). This indicates that the noise patch of 0% coherence dots induced inhibitory interactions between the probe patch and the noise patch, not additional excitation. This could result from divisive normalization (Britten and Heuer 1999) and/or surround suppression (Allman et al. 1985a,b) observed within and/or around RFs of MT neurons. On the other hand, the response at the RF center for the null direction initially showed a small increase, followed by a small decrease when larger noises were presented (Fig. 4*B*, filled triangle). The responses that were measured when the noise patch was presented alone also showed an initial increase followed by a decrease in firing rates (Fig. 4*B*, open square).

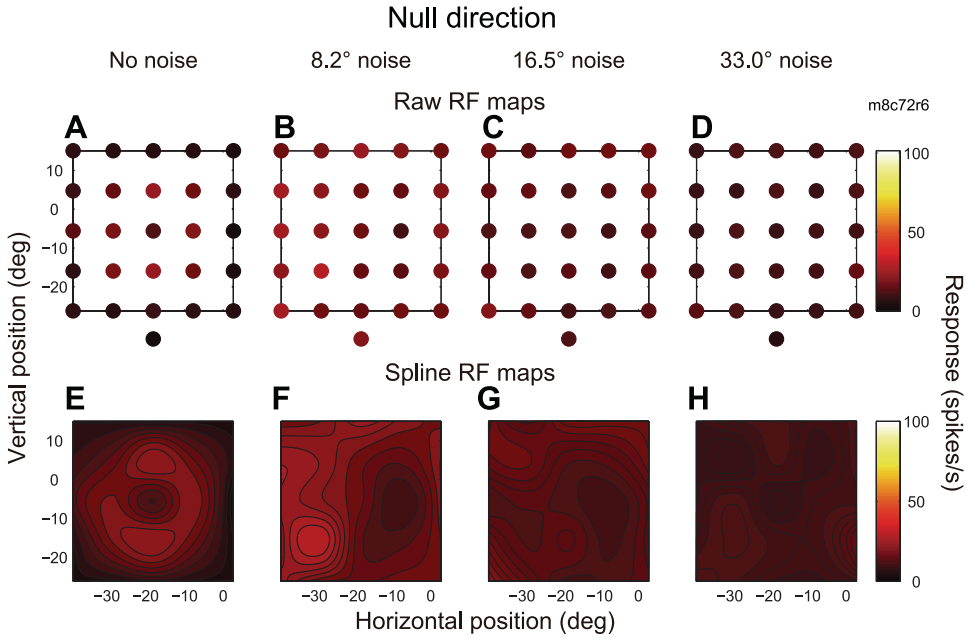

Fig. 3. Raw RF maps (*A–D*) and the spline RF maps (*E–H*) obtained with the null direction for the same neuron as in Fig. 2. Conventions and the color scale of the responses are the same as in Fig. 2.

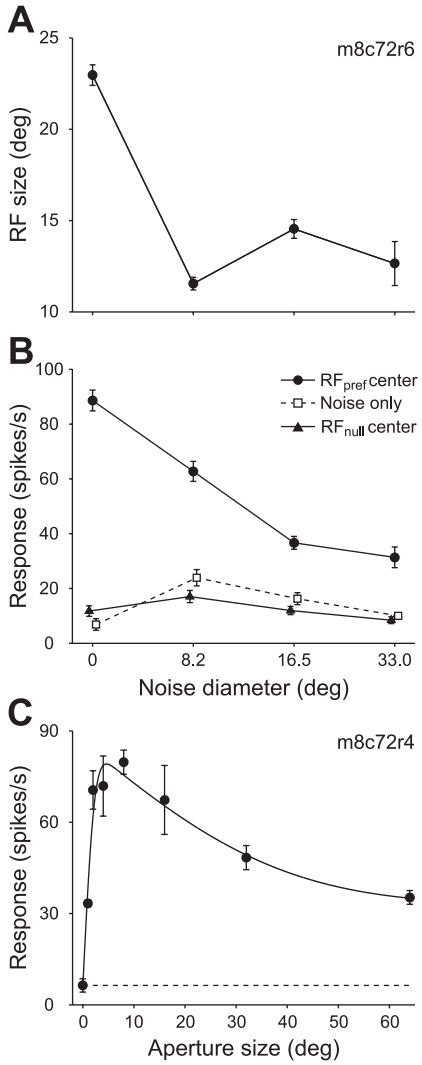

Fig. 4. *A*: RF size, calculated as the square root of the RF area, was plotted against noise diameter. Error bars denote the 95% confidence interval. *B*: response at the RF center for the preferred direction (filled circle), the response at the RF center for the null direction (filled triangle), and the responses to noise patches (open square) were plotted against noise diameter. Error bars denote the SE. Some error bars are smaller than the symbol. *C*: size tuning (area summation) curve of this neuron. Mean firing rates were plotted against the aperture diameter. Error bars denote the SE. Smooth curve is the fitted difference of error function.

This pattern of responses is basically consistent with the size-tuning (area summation) curve of this neuron measured using 100% coherent motion of the preferred direction (Fig. 4*C*). Because MT neurons have recently been shown to exhibit stronger surround suppression for weaker motion stimuli (Hunter and Born 2011), these two response curves should differ quantitatively. We cannot, however, quantify surround suppression with 0% motion coherence stimuli in our study because of the small number of noise patches examined (up to four) for each neuron: thus we cannot be confident whether surround suppression was stronger for weaker motion stimuli compared with those using 100% coherent motion.

The example neuron shown in Figs. 2 and 3 is typical of the MT population. To summarize the apparent RF size contractions, the RF size at each noise condition was normalized to the RF size without noise. Because the exact values of the noise diameter, in degrees of visual angle, were different across neurons, the noise diameter was expressed as a multiple of the RF radius (σ of the fitted two-dimensional Gaussian function) for each neuron. Figure 5*A* summarizes the dependence of normalized RF sizes on noise diameter across the whole population ($N = 135$). Although individual data points were heavily scattered (open circles), the geometric mean of normalized RF sizes across neurons progressively decreased when larger noise patches were presented, and then remained constant at ~40% contraction (filled red circles). We compared the normalized RF sizes between successive noise diameter conditions, and found a statistically significant difference between the no noise condition and the 0.8σ noise condition ($p = 1.47 \times 10^{-7}$, Wilcoxon signed-rank test). All other comparisons did not reach statistical significance. Thus a small noise patch well confined inside the RF was sufficient to induce RF contraction.

The responses at the RF center for the preferred direction, those for the null direction, and the responses to noise patches were normalized to the RF-center response for the preferred direction without noise. The median values of these normalized responses are plotted against noise diameter in Fig. 5*B* ($N = 88$). The normalized RF-center response for the preferred direction monotonically decreased with larger noise patches (Fig. 5*B*, filled circle). The normalized RF-center response for the null direction increased when a small noise up to 1.6σ was presented, indicating an excitation by 0% coherent noise. It then decreased with increasing noise diameter (Fig. 5*B*, filled triangle). The responses to noise patches reached a peak at 1.6σ noise and modestly decreased with increasing noise diameter, reflecting surround suppression of MT neurons (Fig. 5*B*, open square). The results confirm that when presented with large noise, the apparent size of the RF of MT neurons contracted, even at the population level.

The largest noise patch we presented well extended beyond the excitatory classical RF. Because about one-half of MT neurons have an inhibitory surround (Allman et al. 1985a,b; Tanaka et al. 1986; Raiguel et al. 1995), the inhibitory surround mechanism may play a role in the apparent contraction of RF sizes. We evaluated the inhibitory surround from a separate measurement of size tuning curves (see Fig. 4*C*). For our population, 57 out of 135 neurons exhibited significant surround suppression ($P < 0.05$, sequential F test). We then divided the neurons into those with surround suppression and those without and compared the geometric mean values of normalized RF sizes for each subpopulation (Fig. 5*C*). Both subpopulations showed RF contraction when presented with noise patches, but the degree of contraction differed between the two groups. A two-way ANOVA on the normalized RF sizes revealed a significant main effect of noise diameters ($p \ll 0.0001$) as well as a significant main effect of surround suppression ($P = 0.01$), with no interaction between the two factors ($P = 0.55$). The lower value of normalized RF size for surround suppressed neurons suggests that inhibitory surrounds may indeed contribute to the apparent contraction of RF sizes.

To further visualize the changes of RF profile due to the presentation of noise patches, we constructed an average RF map across the 88 neurons for both preferred and null directions at each noise condition. For each neuron, we first normalized responses at each grid location by the RF-center response for preferred direction without noise. We then calculated the average of normalized responses across neurons without any rotation or reflection of the RF mapping grid. Cubic spline interpolation was again used to create the averaged spline RF map. A one-dimensional slice of

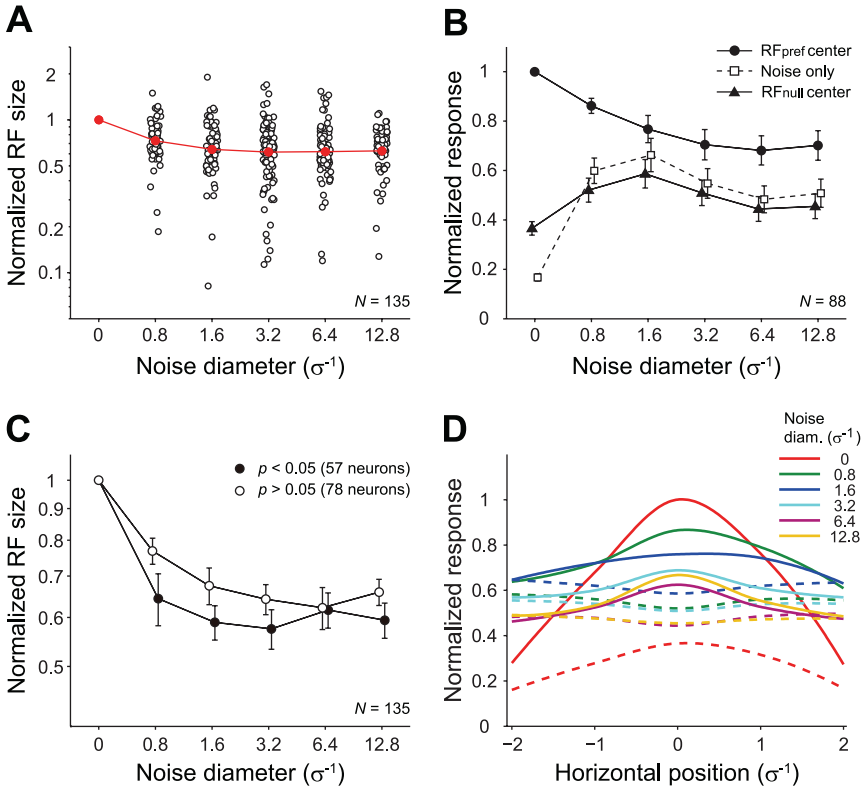

Fig. 5. Changes in RF parameters due to the noise patch were summarized across the MT neuron population. *A*: for each MT neuron, the RF sizes when presented with noise patches were normalized to the RF size without noise. Open circles denote individual values of the normalized RF size. For visualization purpose, the horizontal position of data points within each noise condition was slightly jittered across neurons. Geometric mean values of the normalized RF size across neurons are plotted as red circles. Error bars denoting the SE are smaller than the symbol. *B*: RF-center response for the preferred direction, the RF-center response for the null direction, and the responses to noise patches were normalized to the RF-center response for the preferred direction without noise. Normalized values averaged across neurons are plotted against the diameter of noise patches. Error bars denote the SE. *C*: geometric mean values of the normalized RF size are separately shown for neurons with an inhibitory surround (filled circles) and those without (open circles). *D*: one-dimensional slice of the average RF map is shown across each noise condition. Solid and broken lines denote the RF profile for the preferred and null direction, respectively. Different colors denote RF maps with different noise diameter as shown in *inset*.

these average RF maps through the RF center across directions and noise conditions is shown in Fig. 5*D*. The RF profile without noise for both preferred and null directions (red solid and broken lines, respectively) showed excitatory responses at the RF center relative to those at the RF periphery. When presented with noise patches, the responses at the RF periphery increased from ~0.2 × to ~0.5 × the RF-center response. The RF profile for the null direction with noise can be characterized as an inhibitory interaction. The difference between responses to the preferred and null directions decreased with larger noise, especially at the RF periphery, consistent with a contraction of RF.

Effects of visual noise on direction discriminability of MT neurons. The contraction of RF size (Fig. 5*A*) suggests that MT neurons change their spatial resolution when presented with large distracters. This may come at the cost of a reduced signal-to-noise ratio. We addressed this issue by examining the degree to which the ability of MT neurons to discriminate opposite motion directions was affected by the noise patch. We quantified neuronal performance using the direction-discrimination performance (*d'*) measure. For the majority of the population (88 out of 135), RF maps for the preferred direction (e.g., Fig. 2) and those for the null direction (e.g., Fig. 3) were available. Based on these data, the *d'* at each grid location was calculated as the difference in mean firing rates for the preferred and the null direction divided by the average SD of the firing rates for the two directions.

The *d'* was calculated at all grid positions across the RF. For the example neuron, a *d'* map was constructed using the 2-D cubic spline interpolation (Fig. 6). In these maps, *d'* values were color coded. The area of the *d'* map enclosed by the cyan line was calculated as the area that exceeded half the peak *d'* value. We also extracted the raw *d'* value at the RF center for each noise condition as the discrimination performance of individual MT neurons. The *d'* map of the example neuron contracted when larger noise patches were presented, consistent with the contraction of the RF size. The center *d'* value decreased from 8.08 (without noise) to 4.00 (at the 16.5° noise) to 2.57 (at the 33.0° noise).

To observe the effects of noise diameter on the *d'* map across populations, for each neuron, the size of the *d'* map with noise was normalized to the size of the *d'* map without noise. Geometric mean values of the normalized size were plotted against noise diameter in Fig. 7*A* (red solid circles). The size of *d'* maps gradually decreased down to 38% contraction at 3.2σ

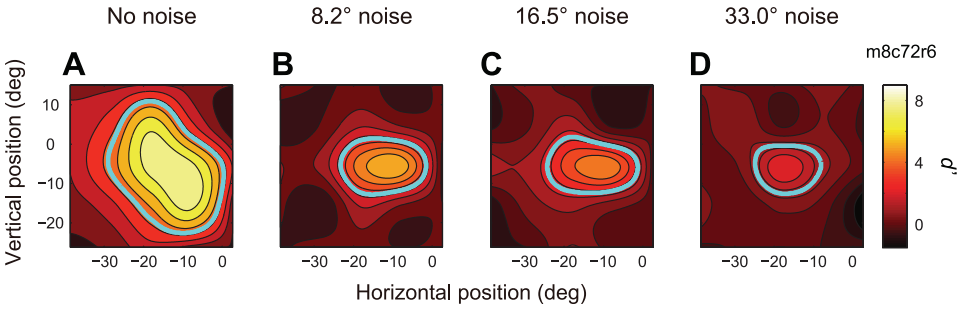

Fig. 6. Neural performance of direction discrimination in the example neuron. The direction-discrimination performance (*d'*) values were calculated at each grid location from the raw RF maps for the preferred direction (Fig. 2, *A–D*) and for the null direction (Fig. 3, *A–D*). Resulting maps were interpolated using a 2-D cubic spline function to construct spline *d'* maps (*A–D*). Cyan lines encompass the area in which *d'* values exceed half the peak *d'* value.

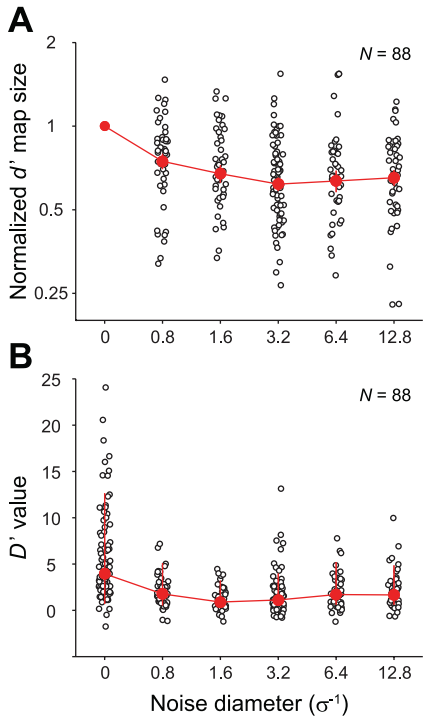

Fig. 7. Changes in *d'* maps due to the noise patch were summarized across the population of MT neurons. *A*: normalized size of the *d'* map for individual data are plotted as open circles. Geometric mean values of the normalized size of the *d'* map across neurons are plotted as red circles. Error bars denote the SE. *B*: The *d'* values at the RF center for individual data are plotted as open circles. The median *d'* value at the RF center across neurons is plotted as red filled circles. Error bars denote the 25 and 75 percentiles. For *A* and *B*, the horizontal position of data points within each noise condition was slightly jittered across neurons.

noise and then slightly increased at the largest noise of 12.8σ. On the other hand, the median center *d'* value of 3.9 decreased to 0.89 when a 1.6σ noise patch was presented (Fig. 7*B*, red solid circles). With larger noise, the center *d'* value recovered to 1.7. The difference in the center *d'* values between 1.6σ noise and 12.8σ noise was statistically significant ($P = 0.0495$, Mann-Whitney *U*-test). The results show that when presented with large noise, the apparent contraction of RF size is accompanied with a reduction in the area sensitive to motion, confirming the notion that motion information in the surrounding region is indeed filtered out. Sensitivity to motion at the RF center was reduced by a factor of ~4, indicating that the signal-to-noise ratio was compromised due to noise and/or RF contraction. However, a slight improvement of the *d'* value at the largest noise size argues for a compensation mechanism that works to counteract the decrease in sensitivity that accompanies the improvement in spatial resolution. This seems to be achieved by a reduction in response especially to the null direction at large noise diameters.

Reduced RF amplitude contributes to RF contraction. Our results showed that when presented with noise patches, both the apparent contraction of RF sizes (Fig. 5*A*) and the reduction of RF amplitude (Fig. 5*B*) occurred simultaneously, at least at the population level. The apparent contraction of RF size thus might have been caused by reduced RF amplitude due to elevated responses at the RF edges and/or the weakened peak response. We therefore examined whether elevated baseline response, weakened peak response, or the combination of the two had a significant relationship with the apparent contraction of RF size.

Figure 8 shows the relationship between RF contraction and the parameters described above. We assessed RF contraction by using the normalized RF size (the ratio of the RF size with noise to the RF size without noise). Because two or three diameter values of noise patches were used for each neuron, the number of normalized RF size values was larger than the number of neurons (376 values from 135 neurons). The median value of the normalized RF size was 0.68, indicating 32% contraction. The elevated baseline response was quantified as the difference in the responses to the noise patch alone and the spontaneous firing rates without noise. The median value of RF baseline difference was 20.7 spikes/s, suggesting excitation by the noise patch. A statistically significant negative correlation was found between normalized RF size and RF baseline difference (Fig. 8*A*; $r = -0.16$, $P = 0.0018$), suggesting that elevated baseline response had an effect on RF contraction. At a RF baseline difference of zero, the normalized RF size was 0.72 {95% prediction interval (PI) was [0.68 0.77]}. This indicates that even in cases where baseline response did not change, 28% RF contraction was observed. The difference in the peak response with and without noise had a median value of −22.4 spikes/s, indicating response suppression due to the noise patch. We found no correlation between normalized RF size and RF peak difference (Fig. 8*B*; $r = -0.05$, $P = 0.33$). The normalized RF size at RF peak difference of zero was 0.63 (95% PI was [0.59 0.66]). We finally examined the difference in the RF amplitude (the peak value minus the spontaneous firing rate or response to noise) with and without noise. The median RF amplitude difference of −49.6 spikes/s suggests a substantial decrease in RF amplitude. Figure 8*C* shows a statistically significant positive correlation between normalized RF size and RF amplitude difference ($r = 0.14$, $P = 0.006$). The normalized RF size at no RF amplitude difference was 0.73 (95% PI was [0.67 0.79]), suggesting that significant contraction of RF size was observed even without a change in RF gain. These results indicate that RF contraction was indeed stronger when RF amplitude was smaller due to baseline elevation. RF contraction, however, was observed even in the absence of reduced RF amplitude.

The lack of a correlation between normalized RF size and RF peak difference (Fig. 8*B*) suggests that the reduced peak response due to suppressive influences when presented with noise patches alone do not contribute to RF contraction. This, at first glance, is inconsistent with our finding that neurons with surround suppression had stronger RF contraction (Fig. 5*C*). We thus quantified the strength of surround suppression from the size-tuning curve for the whole population and examined the relationship between the normalized RF size and the percentage of surround suppression. Although no correlation was found between these two measures collectively (Fig. 8*D*; $r = -0.07$, $P = 0.16$), when we excluded the data points with no surround suppression from the analysis, a significant negative correlation was observed ($r = -0.15$, $P = 0.006$). Thus surround suppression seems to have an effect, albeit weak, on the contraction of RF size.

Contribution of spatial summation mechanisms. We initially used probe and noise stimuli that were not transparent with each other to examine the RF size modulation in situations where a central target was surrounded by distracters. However,

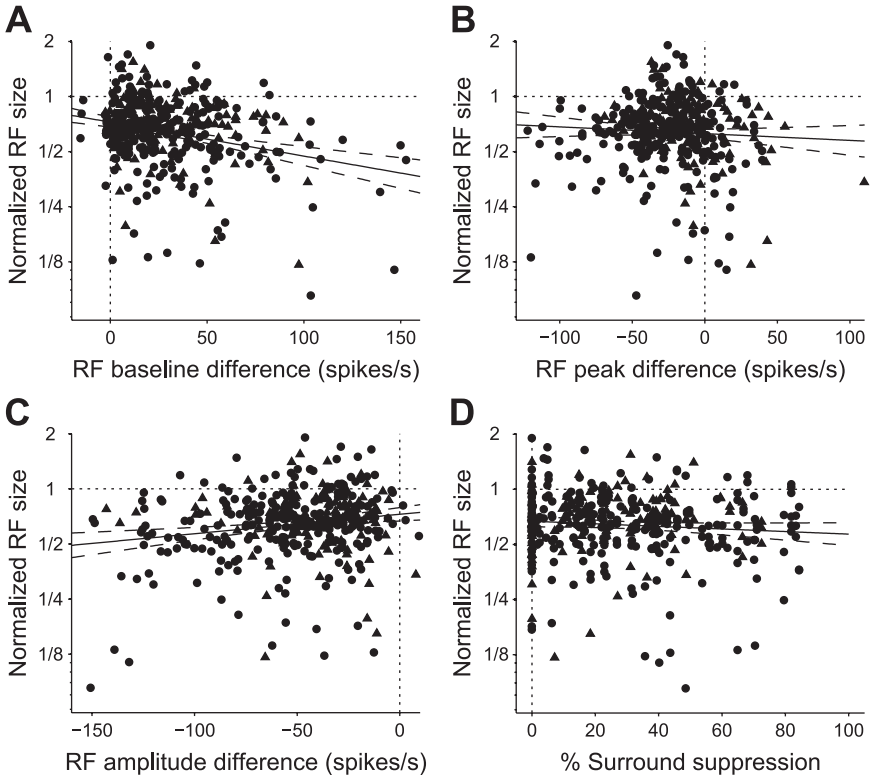

Fig. 8. *A*: normalized RF sizes (the ratio of RF size with and without noise) are plotted against the elevated baseline responses. There was a significant negative correlation between the two. *B*: no correlation was found between the normalized RF sizes and the difference of peak response with and without noise. *C*: normalized RF sizes are plotted against the difference of RF gain with and without noise (abscissa). There was a significant positive correlation between the two. *D*: there was no correlation between the normalized RF sizes and the percentage of surround suppression calculated from the size-tuning curve. Solid and dashed lines in *A–D* indicate the regression line and associated 95% prediction interval.

this stimulus configuration made it difficult to probe mechanisms that underlie the apparent contraction of RF sizes. We thus collected additional data from 27 neurons from *monkey P* in which the probe and noise stimuli were transparent. At least 10 neurons were examined for each noise condition. With this procedure, we first addressed whether RF contraction occurred using this stimulus configuration and then assessed the degree to which spatial summation properties within the RF can account for the apparent contraction of RF sizes.

Figure 9 shows spline RF maps for an example neuron, constructed from raw RF maps and various models. Consistent with data for the original experiment, the apparent sizes of spline RF maps for the two noise conditions were smaller than that without noise (see cyan lines in Fig. 9*A*). The RF size of this neuron without a noise patch was 7.35°. When noise patches of 19.8° and 39.7° (correspond to 6.4σ and 12.8σ) were presented, the RF size contracted to 6.26° and 5.67°. Across the population, the geometric mean of normalized RF sizes steadily decreased toward 0.55 at the largest noise diameter (Fig. 10, filled circles). The result suggests that RF size contracted when presented with noise patches irrespective of whether the probe and the noise were transparent or not.

We assessed the degree to which various versions of spatial summation models (*Eq. 4*; Britten and Heuer 1999; Heuer and Britten 2002; Ghose and Maunsell 2008; Oleksiak et al. 2011) can explain RF contraction obtained with the transparent experiment. The two parameters of the model, a and n, control the spatial summation characteristics. As in Britten and Heuer (1999), we tested a scaled linear model (a is free, $n = 1$), a winner-take-all model ($a = 1$, $n = 100$), a scaled power-law summation or full model (a and n are free), and summation followed by squaring or the Simoncelli-Heeger model (a is free, $n = 0.5$). Each fit was performed by constraining the appropriate parameters as described above, and the optimal parameters were obtained. With the use of the fitted responses, the spline RF maps for the example neuron for each model were constructed and shown in Fig. 9, *B–E*. Not surprisingly, the best account of the data for this example neuron was obtained by the full model in which both parameters were free, resulting in a R^2 of 0.62. Other models had R^2 values ranging from 0.53 to 0.59.

For each model, the RF size was calculated using identical methods as that from raw responses. Normalized RF size values are shown at the *top right* of each RF map (Fig. 9, *A–E*). Consistent RF contractions at the two noise diameters were observed for the full model and the winner-take-all model but not for the others. The profiles of iso-response contours for all models other than the winner-take-all model were basically identical to the contours of the RF without noise. This is due to the formulation of the normalization model (*Eq. 4*) in which the influence of noise is constant across space. In the winner-take-all model, when responses to the RF fringe were smaller than the responses to noise, combined responses were clipped at the level of the noise responses. Accordingly, the apparent size of the winner-take-all model RF contracted when responses to noise were sufficiently strong.

In general, all models provided poor accounts of the data. The example neuron shown in Fig. 9 was one of the best examples whose RF profiles were reasonably well fit by each model. Across the population, the median R^2 values ranged from 0.25 to 0.34, mainly because the models did not reproduce the contraction of apparent RF sizes at large noise diameters (Fig. 10 open symbols). Again, the best account of the data across the population was obtained by the full model, but it only yielded a median R^2 of 0.34. At a noise diameter of 0.8σ, the RF size of the winner-take-all model contracted even

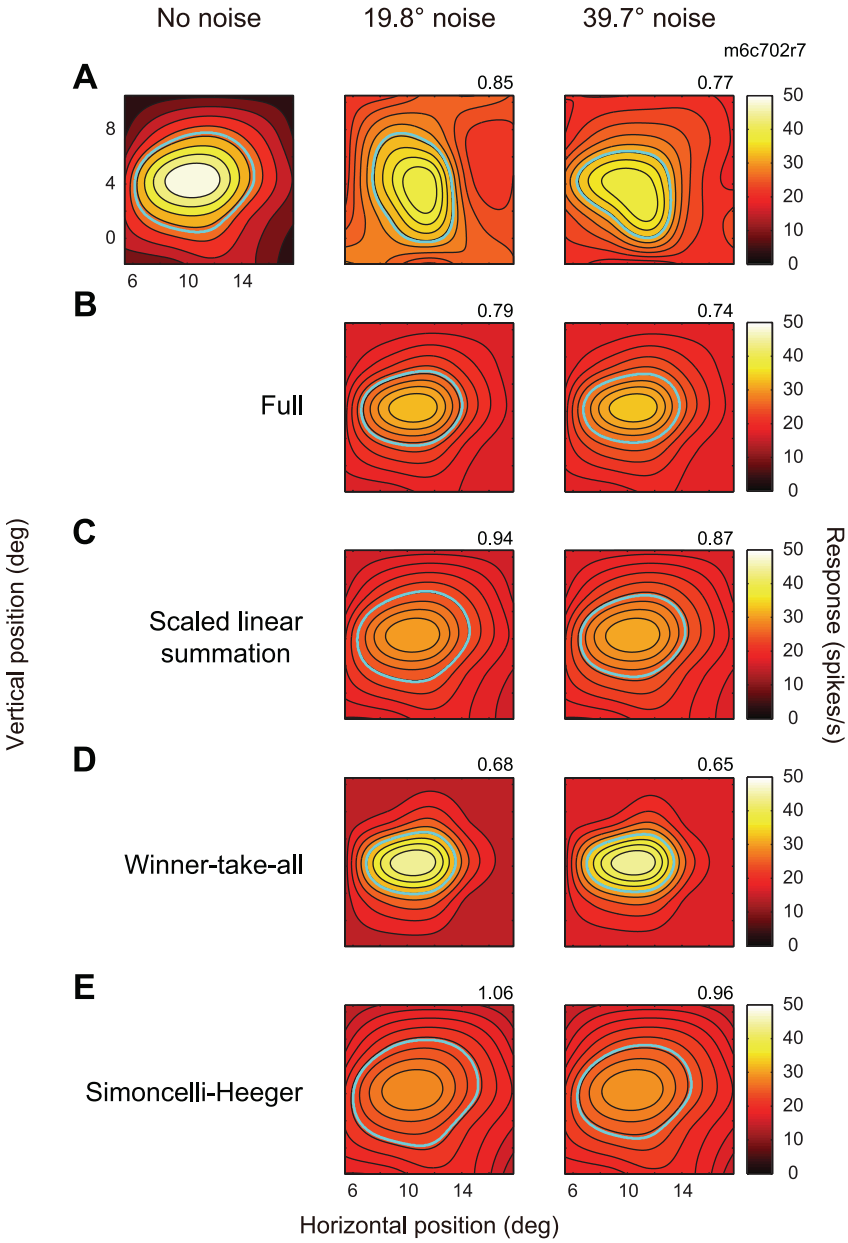

Fig. 9. An example MT neuron showing contraction of the apparent RF size examined with transparent probe and noise patches. *A*: spline RF maps for the preferred direction for three different noise conditions. Noise-patch diameters are written at the *top* of each RF map. Cyan lines are the circumference of the RF area that exceeds half the peak-response modulation. *B–E*: Spline RF maps were created using the responses of the best fit of each version of the response normalization model. Normalized RF size values are shown at *top right*. R^2 values were 0.62 for the full model, 0.59 for the scaled linear summation model, 0.59 for the winner-take-all model, and 0.53 for the Simoncelli-Heeger model. Color scales of the RF map responses are identical across *A–E*.

more than the experimentally observed RF sizes. No model predicted RF contraction comparable to experimental data at noise diameters larger than 6.4σ. We also constructed *d'* maps for the transparent data set. Consistent with the original data set, the size of *d'* maps gradually decreased down to 47% contraction at 12.8σ noise (Fig. 10*B*). The *d'* map constructed from each model response, however, showed modest contraction. From these results, we suggest that the winner-take-all mechanism within the RF is consistent with the apparent contraction of RF sizes when presented with small noise patches but not with large noise patches extending well beyond the RF.

DISCUSSION

In this study, we examined spatial integration properties of MT neurons by using the MRF method. When visual noise was presented within the RFs of MT neurons, the apparent RF sizes decreased to ~60% of those without noise. The results are consistent with a recent finding that showed that spatial summation of MT neurons decreases for low motion coherence (Hunter and Born 2011). RF contraction was accompanied by a reduction in the area sensitive to motion, indicating that the spatial resolution for motion discrimination also increased. Although sensitivity to motion at the RF center decreased with noise, we found a weak recovery of direction discriminability when the largest noise was presented, implying that a compensatory mechanism may work to increase sensitivity in a cluttered visual scene. RF contraction can be explained by a winner-take-all version of the response normalization model at small noise diameters. At large noise diameters, surround suppression might have an additional effect on apparent RF size, although we do not know the exact impact of surround suppression on the degree of RF contraction. Taken together, our results show that spatial resolution improved when confronted with a scene containing high-contrast noise.

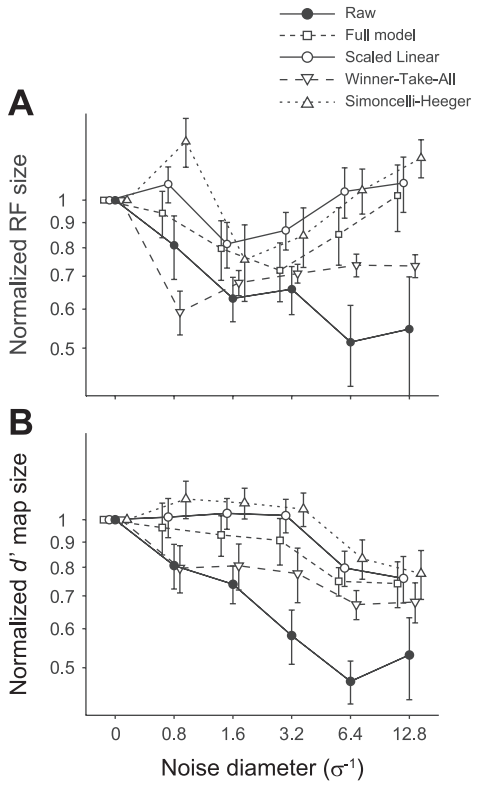

Fig. 10. *A*: geometric mean values of the normalized RF size across neurons for the transparent experiment are plotted as filled circles. Open symbols are corresponding values obtained from the fitted RF of each version of the response normalization model as denoted in the inset. Error bars denote the SE. *B*: geometric mean values of the normalized *d'* map size across neurons for the transparent experiment are plotted as filled circles. Open symbols are corresponding values obtained from the fitted *d'* map of each version of the response normalization model.

Relationship to previous studies. A growing body of evidence suggests that the RF of visual cortical neurons is not static but is a dynamic entity that depends on various factors such as sensory context. The spatial summation of V1 neurons increases with decreasing stimulus contrast (Kapadia et al. 1999; Sceniak et al. 1999; Cavanaugh et al. 2002). Similar findings have been reported for area V2 (Shushruth et al. 2009) and area MT (Pack et al. 2005; Hunter and Born 2011). Thus a dynamic change in spatial summation depending on stimulus contrast is a ubiquitous property observed in various areas of the visual cortex. Additionally, Kapadia et al. (1999) measured length tuning when a bar stimulus was surrounded by a texture background. The texture background induced the same effects as lowering stimulus contrast and increased length tuning. This result is in marked contrast to our results, where RFs contracted when presented with visual noise. This difference might be attributable to differences in the RF measurements (e.g., they did not examine the effects of the texture background on the MRF) and/or to the location of the noise/texture stimuli (texture stimuli were presented in the surround and not at the center). Nonetheless, RF dynamics due to changes in stimulus conditions have been observed repeatedly using the summation method.

Conversely, effects of stimulus condition on MRF measurements are rarely reported. Kapadia et al. (1999) examined the MRF for stimuli of varying contrast. Although quantitative comparisons were not made, they reported that the difference in MRF size between high and low contrasts was small. Gilbert and colleagues have argued that stimulating the RF surround of neurons in cat area 17 can induce an increase in the MRF size (Pettet and Gilbert 1992; Das and Gilbert 1995). In these studies, however, the estimate of RF size might have been confounded with a change in response gain. A quantitative measurement of RF profiles using the reverse correlation technique found a change in response magnitude without any change in RF size, depending on stimulation of the RF surround (DeAngelis et al. 1995; also see Borghuis et al. 2003 for comparison of reverse correlation with conventional methods). Thus our present results represent a unique case where the apparent MRF clearly contracts due to changes in stimulus conditions. It should be noted, however, that although our results are based on the MRF method, RF contraction is due to an interaction between a probe stimulus and concurrently presented visual noise.

Possible mechanisms. A neural network model incorporating feedback projections has been proposed to explain center-surround interactions in V1 neurons (Schwabe et al. 2006). According to this model, the fast and large extent of suppressive surround modulation (Bair et al. 2003), which cannot be accounted for by slow-conducting horizontal connections, is due to feedback from extrastriate neurons with large RFs. Feedback signals drive excitatory neurons at the periphery of the RF of a target V1 neuron, which then excite inhibitory interneurons at the RF center of the target neuron, resulting in suppression of responses at the RF center (see Fig. 2, Schwabe et al. 2006). Can these mechanisms account for our results? The apparent contraction of RF size could occur if probe responses at the RF periphery are suppressed by large noise patches. In the model of Schwabe et al. (2006), inhibitory interneurons are driven by excitatory neurons with RFs at a neighboring location through local excitation. The inhibitory interneurons then suppress responses of excitatory neurons at the same location. Assuming that this neural circuit is applicable for MT, noise patches extending well beyond the RF of a target MT neuron ("far surround" in Schwabe et al. 2006) should activate excitatory neurons within and around the RF of the MT neuron, which in turn should drive inhibitory neurons at the RF periphery of the MT neurons. Suppression of responses to the probe at the RF periphery by these inhibitory neurons should result in RF contraction. Simulations using a network model incorporating feedback and lateral excitation of inhibitory neurons should be examined to test this hypothesis.

The feedback mechanism could account for the apparent RF contraction for the largest noise patch. RF contraction was, however, observed for noise patches as small as 0.8σ (Fig. 5*A*), well inside the RF, suggesting that mechanisms operating within the RF might work in parallel. This raises the possibility that spatial summation mechanisms within the excitatory RF are responsible for RF contraction. To test this explicitly, we examined various versions of the spatial summation model used widely in the literature. The model well predicted the responses to pairs of moving stimuli based on the responses to individual stimulus for MT neurons (Britten and Heuer 1999; Heuer and Britten 2002). For small noise diameter well inside the RF ($\sim 0.8\sigma$), the experimentally observed contraction of RF sizes lies within the range of RF contractions obtained by various versions of the spatial summation model. Among these,

only the winner-take-all model exhibited RF contraction when presented with the 0.8σ noise. Thus the winner-take-all mechanism of spatial integration could contribute to RF contraction for small noises. Apparent RF sizes at large noise patches exhibited more contraction than what any model predicted. Because the degree of RF contraction differed between neurons with suppressive surround and those without (Fig. 5*C*), the apparent RF contraction observed for the large noise patches could partly be due to suppressive influence from the RF surround.

Our results suggest that the apparent contraction of RF size is related to elevated baseline response (Fig. 8*A*) and reduced RF amplitude (Fig. 8*C*) when presented with noise patches. The reduced RF amplitude can result from either an elevated baseline or a reduced peak response for the preferred direction, but the latter had no effect on RF contraction (Fig. 8*B*). The winner-take-all mechanism described above is consistent with the effect of baseline elevation on RF contraction. Baseline elevation is due to excitatory responses driven by a portion of noise patches presented within the RF. The strength of excitatory responses to noise patches depends on the balance between excitation and inhibition driven by preferred and null direction signals contained in 0% coherent noise patches, respectively. This so called "motion opponency" is considered to be computed from V1 to MT (Snowden et al. 1991; Qian and Andersen 1994; Simoncelli and Heeger 1998). The motion opponent mechanism is suggested to achieve noise reduction by subtracting (or dividing) opponent motion signals, because noise should equally activate oppositely tuned motion detectors (Bradley and Goyal 2008). MT neurons with weak motion opponency may exhibit stronger responses to 0% coherent noise and achieve the increased spatial resolution to filter out task-irrelevant noise at the cost of noise reduction.

Context-dependent spatial integration. The region over which signals are spatially integrated should depend on context such as viewing environment and task. In a human psychophysical study of direction discrimination using random-dot motion, increased spatial integration was observed for low motion coherence compared with high motion coherence (Watamaniuk and Sekuler 1992). In cases where signals are surrounded by noise, however, smaller regions of integration should be beneficial for filtering out irrelevant noise. To test this idea, Sasaki and Uka (2011) conducted psychophysical experiments using a direction discrimination task in which a central target of moving random dots was surrounded by a noise annulus of varying diameter. They found that discrimination performance first deteriorated and then recovered when the noise diameter increased, suggesting an improvement in spatial resolution. Moreover, our preliminary results suggest that monkeys also exhibit a similar dependence of noise diameter on psychophysical thresholds (Kumano and Uka 2009). Our current results provide a physiological basis for filtering out task-irrelevant noise in this task.

To filter out irrelevant noise, spatial integration must be restricted to a small region. This, in turn, may come at the cost of a reduced signal-to-noise ratio. Indeed, we found that sensitivity to motion is degraded with added noise (Fig. 7*B*). However, discrimination performance only decreased when the noise diameter increased to $1.6 \times$ the RF radius, and it did not worsen, but rather slightly recovered, at larger noise conditions (Fig. 7*B*). Thus there seems to be a compensatory mechanism that works to counteract the decrease in sensitivity with added noise. This is achieved by decreasing the responses to the null direction as the noise diameter increases (Fig. 5*B*). Thus surround suppression can have a double-edged effect on sensitivity. On one hand, reduced response to the preferred direction can lead to reduced sensitivity. Conversely, reduced response to the null direction can lead to enhancement in sensitivity without explicitly changing direction selectivity when presented with noise patches.

How relevant is the stimulus configuration to our results in this study? To answer this question, it may be useful to compare the current results with typical surround suppression. In a typical MT neuron, responses to dots drifting in the preferred direction first increase and then decrease when the size of the aperture containing the dots increases (Pack et al. 2005; Hunter and Born 2011). Responses to the null direction are constantly suppressed and do not change depending on size (Pack et al. 2005). Thus sensitivity to motion first increases and then decreases when the size of the stimulus increases. This has been confirmed psychophysically in humans (Tadin et al. 2003). Although it is not known whether the MRF changes with stimulus size in this case, motion sensitivity decreases at larger stimulus sizes. This is in contrast to our results, where sensitivity slightly increased at larger stimulus sizes. Therefore, our results are specific to the stimulus configuration in which patches of noise are presented simultaneously with the mapping probe.

ACKNOWLEDGMENTS

We thank Sanae Hosotani and Haruyo Kimizuka for technical and surgical assistance.

GRANTS

This work was supported by Grants-in-Aid for Scientific Research on Priority Areas (system study on higher-order brain function) from the Ministry of Education, Culture, Sports, Science and Technology of Japan (18020026 and 20020025; to T. Uka). H. Kumano was supported by a High Technology Research Center Grant from Ministry of Education, Culture, Sports, Science and Technology of Japan.

DISCLOSURES

No conflicts of interest, financial or otherwise, are declared by the author(s).

AUTHOR CONTRIBUTIONS

Author contributions: H.K. and T.U. conception and design of research; H.K. performed experiments; H.K. analyzed data; H.K. and T.U. interpreted results of experiments; H.K. prepared figures; H.K. drafted manuscript; H.K. and T.U. approved final version of manuscript; T.U. edited and revised manuscript.

REFERENCES

Allman J, Miezin F, McGuinness E. Direction- and velocity-specific responses from beyond the classical receptive field in the middle temporal visual area (MT). *Perception* 14: 105–126, 1985a.

Allman J, Miezin F, McGuinness E. Stimulus specific responses from beyond the classical receptive field: neurophysiological mechanisms for local-global comparisons in visual neurons. *Annu Rev Neurosci* 8: 407–430, 1985b.

Bair W, Cavanaugh JR, Movshon JA. Time course and time-distance relationships for surround suppression in macaque V1 neurons. *J Neurosci* 23: 7690–7701, 2003.

Borghuis BG, Perge JA, Vajda I, van Wezel RJA, van de Grind WA, Lankheet MJM. The motion reverse correlation (MRC) method: a linear systems approach in the motion domain. *J Neurosci Methods* 123: 153–166, 2003.

Bradley DC, Goyal MS. Velocity computation in the primate visual system. *Nat Rev Neurosci* 9: 686–695, 2008.

Britten KH, Heuer HW. Spatial summation in the receptive fields of MT neurons. *J Neurosci* 19: 5074–5084, 1999.

Cavanaugh JR, Bair W, Movshon JA. Nature and interaction of signals from the receptive field center and surround in macaque V1 neurons. *J Neurophysiol* 88: 2530–2546, 2002.

Das A, Gilbert CD. Receptive field expansion in adult visual cortex is linked to dynamic changes in strength of cortical connections. *J Neurophysiol* 74: 779–792, 1995.

DeAngelis GC, Anzai A, Ohzawa I, Freeman RD. Receptive field structure in the visual cortex: does selective stimulation induce plasticity? *Proc Natl Acad Sci USA* 92: 9682–9686, 1995.

DeAngelis GC, Uka T. Coding of horizontal disparity and velocity by MT neurons in the alert macaque. *J Neurophysiol* 89: 1094–1111, 2003.

Efron B. Bootstrap methods: another look at the jackknife. *Ann Stat* 7: 1–26, 1979.

Fitzpatrick D. Seeing beyond the receptive field in primary visual cortex. *Curr Opin Neurobiol* 10: 438–443, 2000.

Ghose GM, Maunsell JHR. Spatial summation can explain the attentional modulation of neuronal responses to multiple stimuli in area V4. *J Neurosci* 28: 5115–5126, 2008.

Heuer HW, Britten KH. Contrast dependence of response normalization in area MT of the rhesus macaque. *J Neurophysiol* 88: 3398–3408, 2002.

Hunter JN, Born RT. Stimulus-dependent modulation of suppressive influences in MT. *J Neurosci* 31: 678–686, 2011.

Judge SJ, Richmond BJ, Chu FC. Implantation of magnetic search coils for measurement of eye position: an improved method. *Vision Res* 20: 535–538, 1980.

Kapadia MK, Westheimer G, Gilbert CD. Dynamics of spatial summation in primary visual cortex of alert monkeys. *Proc Natl Acad Sci USA* 96: 12073–12078, 1999.

Kumano H, Uka T. Change of spatial resolution of direction discrimination: Comparison of MT neuronal and psychophysical performance. *Soc Neurosci Abstr* 558.12, 2009.

Kumano H, Uka T. The spatial profile of macaque MT neurons is consistent with Gaussian sampling of logarithmically coordinated visual representation. *J Neurophysiol* 104: 61–75, 2010.

Lombrozo T, Judson J, MacLeod DIA. Flexibility of spatial averaging in visual perception. *Proc Biol Sci* 272: 725–732, 2005.

Morgan MJ, Ward R. Conditions for motion flow in dynamic visual noise. *Vision Res* 20: 431–435, 1980.

Oleksiak A, Klink PC, Postma A, van der Ham IJM, Lankheet MJ, van Wezel RJA. Spatial summation in macaque parietal area 7a follows a winner-take-all rule. *J Neurophysiol* 105: 1150–1158, 2011.

Pack CC, Hunter JN, Born RT. Contrast dependence of suppressive influences in cortical area MT of alert macaque. *J Neurophysiol* 93: 1809–1815, 2005.

Pettet MW, Gilbert CD. Dynamic changes in receptive-field size in cat primary visual cortex. *Proc Natl Acad Sci USA* 89: 8366–8370, 1992.

Qian N, Andersen RA. Transparent motion perception as detection of unbalanced motion signals. II. Physiology. *J Neurosci* 14: 7367–7380, 1994.

Raiguel S, Van Hulle MM, Xiao DK, Marcar VL, Orban GA. Shape and spatial distribution of receptive fields and antagonistic motion surrounds in the middle temporal area (V5) of the macaque. *Eur J Neurosci* 7: 2064–2082, 1995.

Sasaki R, Uka T. Psychophysical evidence for contraction of the range of spatial integration as a mechanism for filtering out spatial noise in a random dot motion display. *Vision Res* 51: 1979–1985, 2011.

Sceniak MP, Ringach DL, Hawken MJ, Shapley R. Contrast's effect on spatial summation by macaque V1 neurons. *Nat Neurosci* 2: 733–739, 1999.

Schwabe L, Obermayer K, Angelucci A, Bressloff PC. The role of feedback in shaping the extra-classical receptive field of cortical neurons: a recurrent network model. *J Neurosci* 26: 9117–9129, 2006.

Shushruth S, Ichida JM, Levitt JB, Angelucci A. Comparison of spatial summation properties of neurons in macaque V1 and V2. *J Neurophysiol* 102: 2069–2083, 2009.

Simoncelli EP, Heeger DJ. A model of neuronal responses in visual area MT. *Vision Res* 38: 743–761, 1998.

Snowden RJ, Treue S, Erickson RG, Andersen RA. The response of area MT and V1 neurons to transparent motion. *J Neurosci* 11: 2768–2785, 1991.

Tadin D, Lappin JS, Gilroy LA, Blake R. Perceptual consequences of centre-surround antagonism in visual motion processing. *Nature* 424: 312–315, 2003.

Tanaka K, Hikosaka K, Saito H, Yukie M, Fukada Y, Iwai E. Analysis of local and wide-field movements in the superior temporal visual areas of the macaque monkey. *J Neurosci* 6: 134–144, 1986.

Tsui JM, Pack CC. Contrast sensitivity of MT receptive field centers and surrounds. *J Neurophysiol* 106: 1888–1900, 2011.

Uka T, DeAngelis GC. Contribution of middle temporal area to coarse depth discrimination: comparison of neuronal and psychophysical sensitivity. *J Neurosci* 23: 3515–3530, 2003.

Watamaniuk SNJ, Sekuler R. Temporal and spatial integration in dynamic random-dot stimuli. *Vision Res* 32: 2341–2347, 1992.

Womelsdorf T, Anton-Erxleben K, Treue S. Receptive field shift and shrinkage in macaque middle temporal area through attentional gain modulation. *J Neurosci* 28: 8934–8944, 2008.